Biophysical Chemistry 196 (2015) 53–67

Contents lists available at ScienceDirect

Biophysical Chemistry

journal homepage: http://www.elsevier.com/locate/biophyschem

Differentiating antimicrobial peptides interacting with lipid bilayer: Molecular signatures derived from quartz crystal microbalance with dissipation monitoring

Kathleen F. Wang [a], Ramanathan Nagarajan [b,*], Terri A. Camesano [a]

[a] Department of Chemical Engineering, Worcester Polytechnic Institute, Worcester, MA 01609, United States
[b] Molecular Sciences and Engineering Team, Natick Soldier Research, Development and Engineering Center, Natick, MA 01760, United States

HIGHLIGHTS

- Interactions between lipid bilayers and 4 structurally diverse AMPs were examined.
- Each peptide's interaction mechanism produces a unique molecular QCM-D signature.
- QCM-D signatures give information about the dynamics of AMP–membrane interactions.
- Mechanistic variations were related to AMP structural properties (e.g. hydrophobicity).

GRAPHICAL ABSTRACT

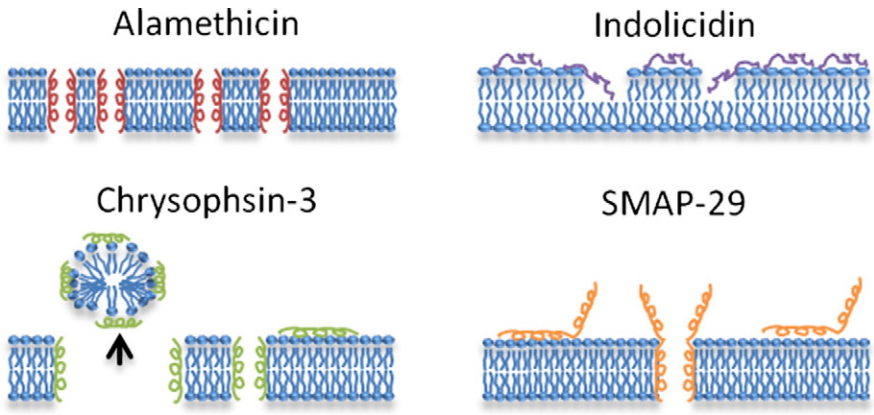

ARTICLE INFO

Article history:
Received 11 September 2014
Received in revised form 16 September 2014
Accepted 16 September 2014
Available online 28 September 2014

Keywords:
Antimicrobial peptide
Supported lipid bilayer
Quartz crystal microbalance
Peptide–bilayer interaction
Peptide structure–activity
Membrane destabilization

ABSTRACT

Many antimicrobial peptides (AMPs) kill bacteria by disrupting the lipid bilayer structure of their inner membrane. However, there is only limited quantitative information in the literature to differentiate between AMPs of differing molecular properties, in terms of how they interact with the membrane. In this study, we have used quartz crystal microbalance with dissipation monitoring (QCM-D) to probe the interactions between a supported bilayer membrane of egg phosphatidylcholine (egg PC) and four structurally different AMPs: alamethicin, chrysophsin-3, indolicidin, and sheep myeloid antimicrobial peptide (SMAP-29). Multiple signatures from the QCM-D measurements were extracted, differentiating the AMPs, that provide information on peptide addition to and lipid removal from the membrane, the dynamics of peptide–membrane interactions and the rates at which the peptide actions are initiated. The mechanistic variations in peptide action were related to the fundamental structural properties of the peptides including the hydrophobicity, hydrophobic moment, and the probability of α-helical secondary structures.
Published by Elsevier B.V.

1. Introduction

Antimicrobial peptides (AMPs) are pathogen-killing molecules that were originally derived from various organisms, including frogs and moths [1,2]. They are known to kill a broad spectrum of pathogenic bacteria, fungi, and viruses. AMPs are believed to kill bacteria by destabilizing bacterial membranes or translocating through the membranes to interact with intracellular targets. Because of the nature of these interactions, pathogenic bacteria are less able to develop resistance against the membrane-active AMPs, in contrast to the ease of

* Corresponding author. Tel.: +1 508 233 6445; fax: +1 508 233 4469.
E-mail address: Ramanathan.nagarajan.civ@mail.mil (R. Nagarajan).

http://dx.doi.org/10.1016/j.bpc.2014.09.003
0301-4622/Published by Elsevier B.V.

developing antibiotic resistance. A bacterium must substantially change the characteristics of its membrane if it has to succeed in developing resistance to AMPs, but because the lipids are highly conserved in microorganisms, this occurrence is unlikely [3–5]. This unusual property of low susceptibility to development of AMP resistance by the microorganisms has stimulated major research efforts to chemically synthesize AMPs replicating some of the structural features of the naturally occurring AMPs, with the expectation of reproducing their mechanism of action in killing bacteria for practical applications.

The membrane-destabilizing mechanisms exhibited by AMPs are thought to fall into several categories. Many membrane-active peptides have been shown to insert into lipid bilayers and create pores using a mechanism described by the barrel-stave model [6]. These pores have been detected by studying voltage-dependent conductance that occurs via transmembrane channels that are created as a result of peptide insertion [7,8]. The AMPs may also disrupt cell membranes by first attaching to the surface and forming lipid–peptide aggregates, which then leave the membrane causing lysis, in a mechanism described by the carpet model. Variations of these models have also been developed. For instance, the barrel-stave cylindrical pores, in which the edges are lined by perpendicularly-oriented peptides, may be distinguished from toroidal pores, in which the pore edges consist of peptides and lipid head groups that bend continuously from the top bilayer leaflet to the bottom bilayer [9]. The mechanism of interaction between a peptide and a cell membrane may follow any one or a combination of these molecular events, depending on the type of peptide and lipid present in the system.

Peptide characteristics of secondary structure, charge, and hydrophobicity are usually thought to play substantial roles in determining AMPs' mechanisms of action on a cell membrane [10]. Studies have shown that increased helicity in AMPs can be correlated with increased antibacterial activity [11,12]. The cationic nature of AMPs is also thought to play a large role in their ability to target negatively charged bacterial cell membranes. Electrostatic interactions are largely responsible for drawing cationic AMPs to anionic bacterial cell membranes. If the membrane is primarily made up of zwitterionic lipids, then the strong ionic attractions that exist between the anionic lipid membranes and the AMP are replaced by relatively weaker attractive interactions between the dipoles of the neutral membrane and the charges on the AMP. In this case, the hydrophobicity of the peptide may become a more significant factor in determining antimicrobial activity. Hydrophobicity has been shown to affect the antibacterial and hemolytic activity of AMPs, but the correlation with antibacterial activity may not be strong [10,13–17]. Although numerous studies in the literature have examined the relationship between AMP structure and antibacterial or hemolytic activity (represented by experimentally determined minimum inhibitory concentrations), less is known about how the structure of the AMP and its resulting physicochemical properties determine the specific mechanism of interaction with cell membranes.

To discover the mechanistic variations between different AMPs, four molecules, alamethicin, chrysophsin-3, indolicidin, and sheep myeloid antimicrobial peptide (SMAP-29), with varying secondary structures, charges, and hydrophobicities were chosen for this study (Table 1). The helical wheel diagrams for these four peptides are shown in Fig. 1. This diagram provides a projection of amino acids perpendicular to the helix long axis assuming that the peptide exists in an α-helical secondary structure. Since the α-helix contains 3.6 residues per turn, adjacent residues on the peptide are separated by 100° on the helical wheel.

The first AMP, alamethicin, is a 20-amino-acid, α-helical peptide that is derived from the fungus *Trichoderma viride* and is known to insert into membranes at higher concentrations, forming well-defined cylindrical pores [18–20]. The structure of alamethicin includes two amino acids that are rarely found in nature, aminoisobutyric acid and L-phenylalaninol. Alamethicin contains a negative charge associated with the glutamic acid residue near the C-terminus. However, this side chain is typically protonated when the peptide is oriented in a transmembrane state, making alamethicin's net charge effectively zero in a peptide–lipid membrane system [21]. The helical wheel diagram shows a clear separation between the dominant hydrophobic face and a smaller polar face in the alpha-helical structure for this peptide.

Chrysophsin-3, another 20-amino-acid AMP, is derived from the gills of the red sea bream, *Chyrsophrys major*. It also assumes an α-helical structure when in contact with a biological membrane and is amphipathic [22,23]. Chrysophsin-3 exhibits a positive net charge of +5 (fractional charge 3.2 at pH 7), which differentiates it from alamethicin. Again in this case, the helical wheel diagram shows a clear separation between the dominant hydrophobic face and a polar charged face in the alpha-helical structure for this peptide.

Indolicidin, a 13-residue AMP derived from bovine neutrophils, is one of the smallest of the known naturally occurring linear peptides [24]. Indolicidin's amino acid content is quite remarkable because of its five tryptophan and three proline residues. Indolicidin carries a net charge of +4 at pH 7 and assumes a specific coiled and folded conformation when in contact with a cell membrane, unlike the α-helical or β-sheet conformations formed by most other AMPs [25,26]. Intramolecular cation–π electron interactions allow it to assume a folded, boat-shaped conformation with positive charges at the peptide termini and a hydrophobic core [27–29]. Studies have shown that indolicidin does not cause hemolytic lysis at concentrations below 30 μM [30]. The helical wheel diagram shows a separation of hydrophobic and hydrophilic residues but the large presence of prolines in this small peptide prevents it from assuming an α-helical secondary structure.

Sheep myeloid antimicrobial peptide (SMAP-29) is a cationic AMP composed of 29 amino acids that carries a +11 net charge at pH 7 [31]. Its structure is predominantly α-helical, with the hydrophobic residues aligned along one side and the polar residues along the other [32–34] as can be seen from the helical wheel diagram. The SMAP-29 used in our study contains a C-terminal cysteine residue, which was introduced to support other research where the AMP was attached to fluorescent dyes or other surfaces through the sulfhydryl functionality of cysteine [35,36]. The presence of the terminal cysteine could possibly give rise to the formation of SMAP dimers in solution through disulfide bonding.

In addition to the selection of peptides, it is necessary to specify the membrane model, the type of lipids and the experimental technique to explore the AMP–membrane interactions. In the literature, different membrane models and experimental techniques have been reported, each technique providing useful observations about one or another aspect of the AMP interactions, making it necessary for multiple techniques to be applied to piece together a comprehensive molecular scale picture of the AMP action. For example, the AMP alamethicin has been studied using black lipid membranes, vesicles, liposomes, multilayers, and Langmuir–Blodgett film as membrane models, prepared with different choices of lipid molecules and employing experimental techniques including electrical conductance [37], crystallographic analysis [38], circular dichroism [39], phenylalaninol fluorescence [39], oriented circular dichroism (OCD) [19], neutron in-plane scattering [40], X-ray diffraction [41], cryo transmission electron microscopy (cryoTEM) [42], liposome leakage measurements [42], electrochemical scanning tunneling microscopy [43] and also computer simulations [43-45].

Because of its real time monitoring capability, we employed quartz-crystal microbalance with dissipation monitoring (QCM-D) as the technique on the membrane model of solid supported lipid bilayer (SLB), to monitor the dynamics of AMP–membrane interactions and to search for molecular signatures specific to each peptide. With QCM-D, changes in mass and viscoelasticity of a supported lipid bilayer can be quantitatively determined by monitoring the changes in frequency (Δf) and energy dissipation (ΔD) of a quartz crystal sensor on which the bilayer is assembled [46–52]. Due to varying acoustic penetration depths of the different overtones [46], higher overtones are correlated with processes occurring closer to the sensor surface [46] while the lower overtones

Table 1
Characteristics of various antimicrobial peptides.

Peptide	Number of amino acids	Predominant secondary structure[a]	Nominal charge at pH 7	Comments
Alamethicin[b] Ac-UPUAUAQUVUGLUPVUUEQZ	20	α-helix [38]	0 [21]	Contains non-proteinogenic amino acids aminoisobutyric acid and phenylalaninol
Chrysophsin-3 H-FIGLLISAGKAIHDLIRRRH-OH	20	α-helix [22]	+5	
Indolicidin H_2N-ILPWKWPWWPWRR-OH	13	Folded, boat-shaped conformation [29]	+4 [26]	Smallest peptide with dominant presence of tryptophan and proline
SMAP-29 H_2N-RGLRRLGRKIAHGVKKYGPTVLRIIRIAG-OH	29	α-helix [32]	+11	Cysteine was attached at the C-terminus to support other research

[a] The secondary structures mentioned in the literature for the peptides in aqueous solutions, when in contact with biological membranes.
[b] "U" and "Z" represent the non-proteinogenic amino acids α-aminoisobutyric acid and L-phenylalaninol, respectively. N- and C-terminal groups are also shown on each amino acid sequence.

represent processes occurring closer to the aqueous interface. The measurements can be made at multiple frequency overtones, or harmonics, and related to homogeneity of molecular processes occurring through the depth of the bilayer, following the overtone analysis pioneered by Mechler et al. [47]. QCM-D also offers information on the dynamics of the process because of the real time monitoring of very small mass and dissipation changes.

In selecting the lipids for the membrane model, our choice was influenced by the need to study both the antimicrobial action of AMPs and the hemolytic action of AMPs. Egg phosphatidylcholine (egg PC) bilayers and vesicles have been used extensively to model erythrocyte membranes and egg PC and other zwitterionic phospholipids have also been shown to form highly reproducible supported lipid bilayers (SLBs) [50–52]. Therefore, for all the experiments reported in this paper, we used egg PC as the lipid. Bacterial membranes have either all anionic lipids (Gram-positive bacteria) or a mixture of anionic and zwitterionic lipids (Gram-negative bacteria) [53]. The successful formation of robust and stable SLBs with a large proportion of anionic lipids (such as phosphatidyl glycerol, PG and lysophosphatidyl glycerol, LPG) has not yet been achieved. Our lab has recently made progress in developing protocols for first treating the quartz surface and then forming SLBs composed of only anionic lipids. We plan to use such anion dominant membrane models representing bacterial cells in future studies.

Specific molecular structural characteristics of each AMP, such as charge, α-helicity, hydrophobicity and hydrophobic moment were calculated and combined with the molecular signatures derived from QCM-D to relate peptide molecular structural characteristics with the mechanism of how the AMP interacts with the lipid bilayer.

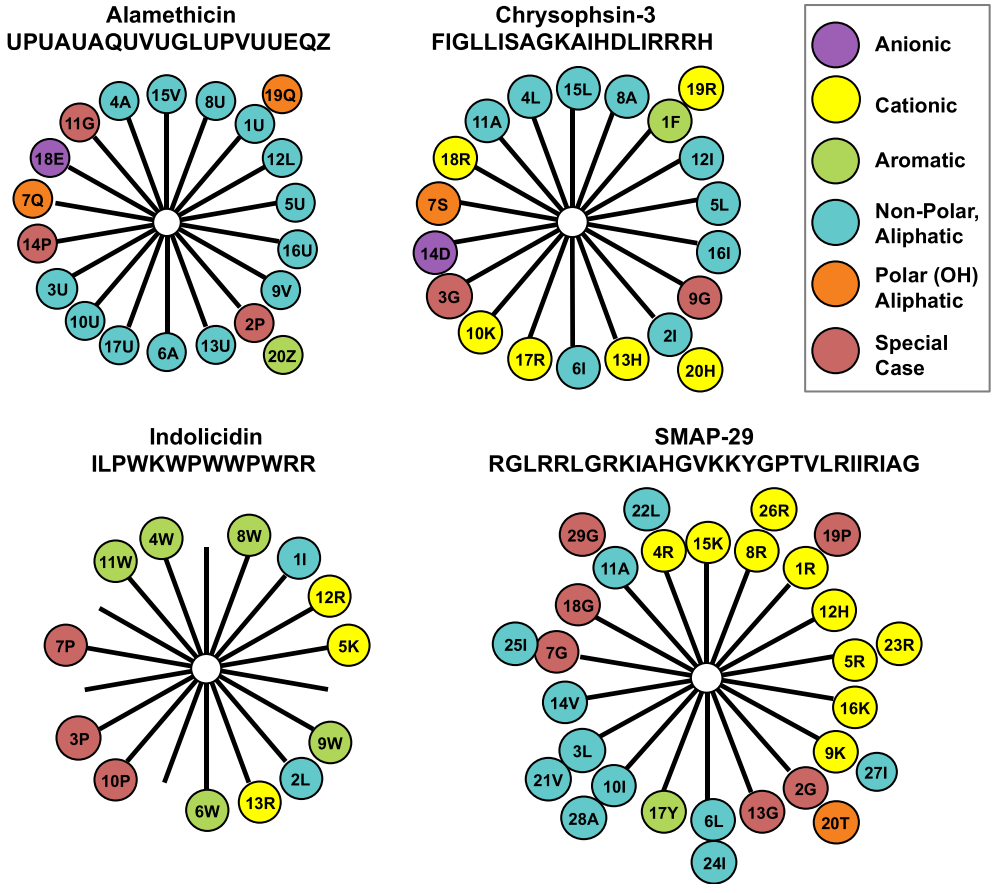

Fig. 1. Helical wheel diagrams for alamethicin, chrysophsin-3, indolicidin, and SMAP-29. α-Aminoisobutyric acid and L-phenylalaninol in alamethicin's amino acid sequence are represented by "U" and "Z," respectively. These diagrams reveal differences in the placement of charged amino acid residues, as well as hydrophobic and polar side chains.

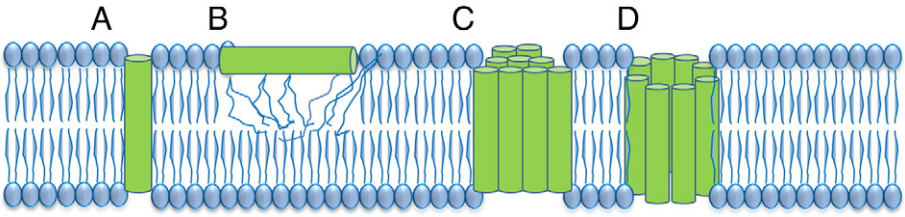

Fig. 2. Four states of peptide–membrane interactions: (A) peptide insertion into the bilayer as a single molecule, (B) peptide adsorption to the membrane surface, (C) peptide insertion as an aggregate without a water channel and (D) peptide insertion as a cluster forming a pore around a water channel.

2. Materials and methods

2.1. Materials

Indolicidin and cysteine-terminated SMAP-29 (cysteine located at the C-terminus) were purchased from New England Peptide (Gardner, MA). Alamethicin was purchased from Sigma-Aldrich (St. Louis, MO) and chrysophsin-3 was acquired from Bachem (Torrance, CA). Peptide and lipid vesicle solutions were prepared in Tris–NaCl buffer [100 mM sodium chloride and 10 mM tris(hydroxymethyl)aminomethane at pH 7.8]. All solutions were prepared in Tris–NaCl buffer to facilitate the formation of stable supported lipid bilayers and prevent non-peptide-related changes at the membrane–liquid interface. Lyophilized egg phosphatidylcholine (PC) was purchased from Avanti Polar Lipids (Alabaster, AL) and stored in ethanol at −20 °C.

2.2. Supported lipid bilayer preparation

The stored egg PC was dried with nitrogen gas to remove the ethanol and stored under vacuum in a desiccator overnight. The dried lipids were then resuspended in Tris–NaCl buffer and brought to a final concentration of 2.5 mg/mL. The mixture was subjected to 5 freeze–thaw cycles and small unilamellar vesicles (SUVs) were formed using an ultrasonic dismembrator (Model 150 T, Fisher Scientific, Waltham, MA) in pulse mode for 30 min at 0 °C. The pulse was set to stay on for 3 s at an amplitude of 60, followed by a 7 s pause, resulting in a 30% duty cycle. The SUV solution was then centrifuged at 17,500 rpm (37,000 *g*) for 10 min at 4 °C (J2-MI Centrifuge, Beckman Coulter, Brea, CA). The supernatant containing homogeneous SUVs was collected and stored under nitrogen at 4 °C for up to 5 weeks. This stock solution was aliquoted and diluted to 0.1 mg/mL before each experiment. Experiments were performed with peptide concentrations between 0.5 μM and 10 μM. Lower concentrations between 0.01 μM (data not shown) and 0.5 μM were also tested with alamethicin, chrysophsin-3, and SMAP-29 to determine the critical concentration at which AMP action occurs.

2.3. QCM-D experiments

The Q-SENSE E4 system (Biolin Scientific, Stockholm, Sweden) was used to monitor the formation of an SLB on a silica surface and changes to the membrane upon exposure to AMPs in real-time. This technique uses the piezoelectric qualities of a quartz sensor crystal to measure the relative change in mass on its surface. The instrument measures the change in frequency (Δf) and change in energy dissipation (ΔD) of the crystal and any associated mass.

All the experiments involved the following steps (see a typical trace of frequency and dissipation measurements over time in the Supplemental Material Topic S1). First, at time t_0, a PC vesicle solution (0.1 mg/mL) was allowed to flow over the QCM-D silica sensor surface at 0.15 mL/min until the frequency and dissipation stabilized, indicating the formation of a stable bilayer [50,51]. The vesicles initially attach to the silica surface and then rupture spontaneously forming a stable and uniform membrane. A Viton o-ring positioned around the edge of the silica surface prevented the lipid bilayer from having any lateral areal expansion once formed. Then at time t_1, the buffer was injected into the QCM-D chamber to rinse away any unattached particles. When the system showed a stable response at time t_2, a solution of the AMP in the buffer at the desired peptide concentration was allowed to flow. After 10 min of AMP injection, at time t_3, the flow was stopped and the system was left to equilibrate for 1 h. Following this equilibration step, at time t_4, a final buffer rinse was applied until the frequency and dissipation stabilized at time t_5. The change in frequency Δf and change in dissipation ΔD data reported everywhere in this paper are the difference in values between that at time point t_2 associated with a stable supported bilayer just before AMP injection and the time point t_5 at the end of the final buffer rinse. The differences thus reflect solely the consequences of AMP interaction with the bilayer and are unaffected by all other system variables.

The Δf and ΔD values were measured with the 3rd, 5th, 7th, 9th, and 11th harmonics, or overtones, of the QCM-D crystal's resonant frequency. Due to different penetration depths of the acoustic waves associated with different overtones, higher overtones (e.g. the 9th and 11th harmonics) are associated with activity near the crystal surface and lower overtones are more related to processes occurring near the external surface of the attached mass [47–49]. Homogeneous Δf and ΔD values at all overtones suggest that the process occurs throughout the thickness of the bilayer.

2.4. QCM-D data analysis

Methods to relate the measured frequency and dissipation changes to changes in mass and in the viscoelastic properties of the membrane on the surface are briefly outlined here. For a rigid film on the crystal

Table 2
Calculated estimates of maximum frequency changes resulting from various modes of peptide–bilayer interactions.

Peptide	Molecular weight of peptide (Da)	Expected maximum Δf (Hz)			
		Insertion as monomer or as cluster	Pore formation with 8 peptides/pore	Pore formation with 20 peptides/pore	Surface adsorption flat
Alamethicin	1965	−0.10	6.92	12.08	−4.85
Chrysophsin-3	2287	−3.26	4.91	10.91	−4.85
Indolicidin	1906	0.48	7.29	12.29	−4.85
SMAP-29	3256	−12.78	−1.14	7.41	−4.85
SMAP-29 Dimer	6512	−44.74	−21.47	−4.37	−4.85

surface exposed to air, the areal mass m_f (mass per unit area) is related to the frequency change Δf by the Sauerbrey equation, while the dissipation change ΔD is zero. The frequency value reported by the Q-Sense system is normalized so that the QCM-D output is $\Delta f_n / n$, where Δf_n is the frequency at overtone number n. The ΔD value is not normalized.

$$\Delta f = -f_o \frac{m_f}{m_q} = -C\, m_f, \quad \Delta D = 0 \tag{1}$$

Here, f_o is the natural frequency of the oscillator, m_q is the areal mass of the quartz crystal and C is the Sauerbrey constant. Net mass addition is reflected by a negative Δf (decrease in frequency) while net mass loss is indicated by a positive Δf (increase in frequency). If the film is not rigid but viscoelastic and is submerged in a Newtonian liquid (water or buffer), then the frequency and dissipation changes are given by

$$\Delta f = -\frac{\eta_L}{2\pi\delta_L m_q} - f_o \frac{m_f}{m_q}\left[1 - \frac{2}{\rho_f}\left(\frac{\eta_L}{\delta_L}\right)^2 \frac{G''}{G'^2 + G''^2}\right],$$
$$\Delta D = \frac{\eta_L}{n\pi f_o \delta_L m_q} + \frac{m_f}{m_q}\left[\frac{4}{\rho_f}\left(\frac{\eta_L}{\delta_L}\right)^2 \frac{G'}{G'^2 + G''^2}\right] \tag{2}$$

where ρ_f is the density of the film on the crystal, η_L is the viscosity of the liquid, δ_L is the decay length of the acoustic wave in the liquid, and G'' and G' are the loss modulus and the storage modulus connected to the dissipation, $D = G'' / (2\pi G')$ [46]. The measured Δf value is normalized with the overtone number n (by dividing the frequency value for each overtone by n), while ΔD is not normalized. The first term in the expressions for Δf and ΔD is due to the solvent effect and they vanish when we consider peptide-induced changes in the bilayer since the bilayer is immersed in the liquid both before and after contact with the peptide.

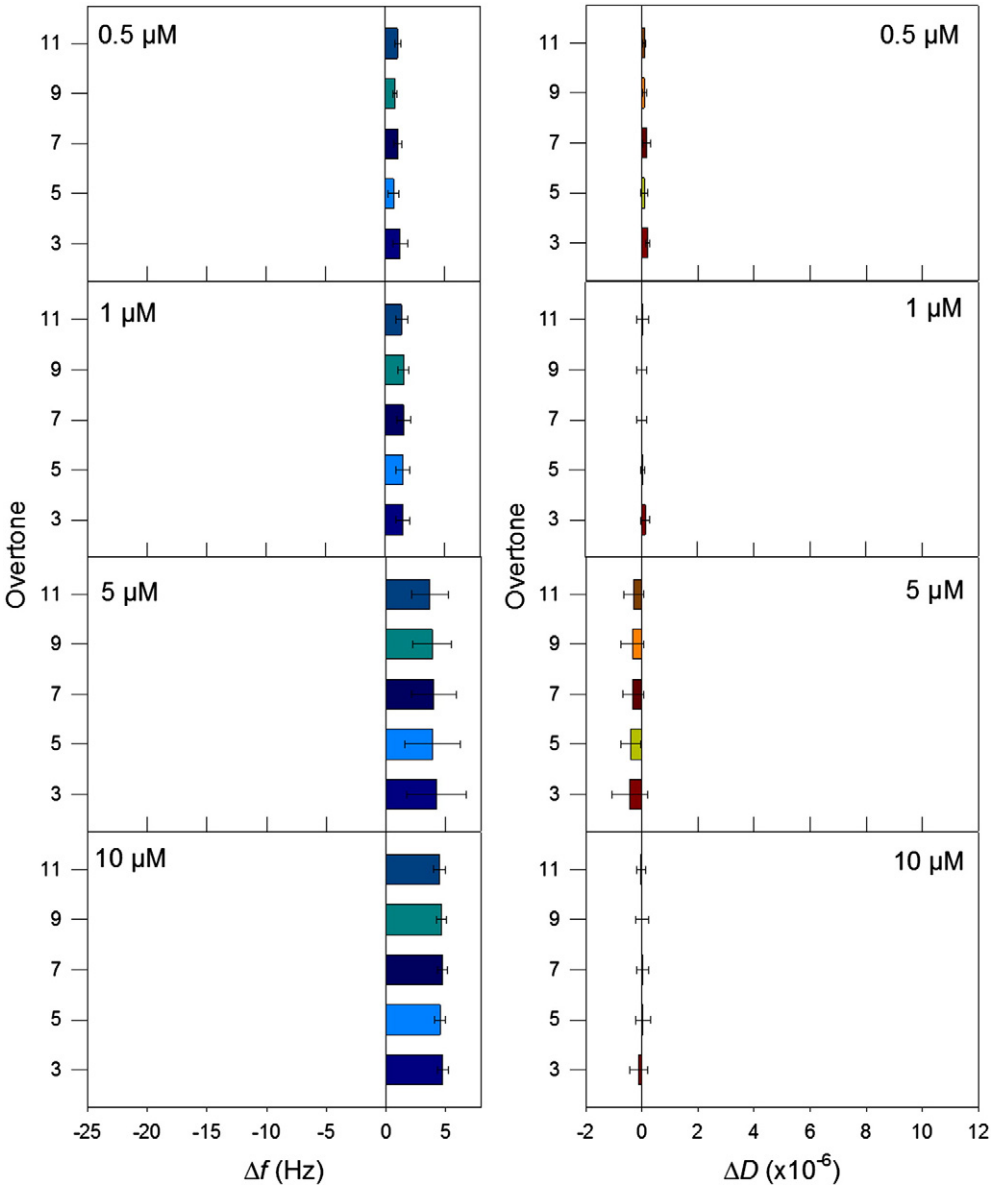

Fig. 3. Changes in frequency and dissipation corresponding to various concentrations of alamethicin interacting with a PC membrane (data previously published) [49]. The uniform increases in frequency and dissipation at all overtones for each peptide concentration point to mass changes throughout the membrane thickness, which are indicative of peptide insertion. Error bars represent the standard deviation based on at least 3 replicate experiments.

The mass change is now given by the Sauerbrey term with a correction factor accounting for the viscoelastic properties of the film. The change in dissipation ΔD is related to the changes in the rigidity or viscoelasticity of the bilayer. Small ΔD implies bilayer rigidity similar to that of the unperturbed bilayer and in this case the mass change is given by the simple Sauerbrey term without the viscoelastic correction.

3. Results and discussion

3.1. Dependence of frequency changes on peptide interaction modes

In order to link the frequency changes measured in the QCM-D experiments to molecular events, we first established a connection between the frequency changes and the different modes of peptide interaction with the bilayer. Four different states of peptide interacting with the membrane are shown in Fig. 2: (A) peptide is inserted into the bilayer as a single molecule, occupying an area a_p per peptide; (B) peptide is adsorbed on the bilayer surface in the lipid head group region, occupying an area A_p; (C) peptide is inserted into the bilayer as an aggregate without any water channel, occupying an area a_p per peptide; and (D) peptide is inserted into the bilayer as a n-size cluster forming the pore wall around a water channel, occupying an area A_H / n per peptide, A_H being the pore cross-sectional area. If the peptide adsorbs on the bilayer surface, there is no need for any lipid removal to occur. On the other hand, if peptide addition results in pore formation or in the insertion of single peptides or peptide aggregates into the bilayer then some lipid molecules will have to be removed from the bilayer since the total bilayer area cannot expand on the quartz crystal. If a fraction λ of the bilayer area is affected by these peptide interactions, then the resulting frequency changes can be calculated (see details in Supplemental Material Topic S2) as the areal mass change divided by the Sauerbrey constant C:

$$\Delta f = -\frac{\lambda}{C}\left[\frac{M_P}{a_P} - 2\frac{M_L}{a_L}\right] \quad \text{Insertion of peptide/peptide clusters}$$
$$\Delta f = -\frac{\lambda}{C}\left[\frac{M_P}{\frac{A_H}{n}} - 2\frac{M_L}{a_L}\right] \quad \text{Formation of pores} \qquad (3)$$
$$\Delta f = -\frac{\lambda}{C}\left[\frac{M_P}{A_p}\right] \quad \text{Adsorption of peptides}$$

In this equation, M_P and M_L are molecular masses of the peptide and lipid molecule, respectively, calculated from their molecular weights.

Setting the fractional area λ to be unity, we have calculated the theoretical maximum in the frequency change (corresponding to $\Delta f_n / n$) and the results are given in Table 2. From the calculated results, we observe that for alamethicin, pore formation will give rise to a positive Δf and will be measurable. In contrast, if alamethicin simply inserts into the bilayer either as a single molecule or as an aggregate, Δf is negative but will be too small to be observed. If alamethicin adsorbs on the bilayer surface with the helix being flat, Δf will be negative and large enough to be observable. For chrysophsin-3, pore formation will give rise to a positive Δf and will be measurable. If the peptide simply inserts into the bilayer or if it adsorbs on the bilayer, the frequency change will be negative and measurable. For indolicidin, pore formation will give rise to a positive Δf and will be measurable. If the peptide simply inserts into the bilayer, Δf will be positive but too small to be measurable. If indolicidin adsorbs flat on the bilayer surface, Δf will be negative and large enough to be observable. For SMAP-29, formation of a large pore will give rise to a positive Δf, while for a small pore Δf will be negative. If the peptide simply inserts into the bilayer, Δf is negative and large enough to be observed. Also, if the peptide is adsorbed flat

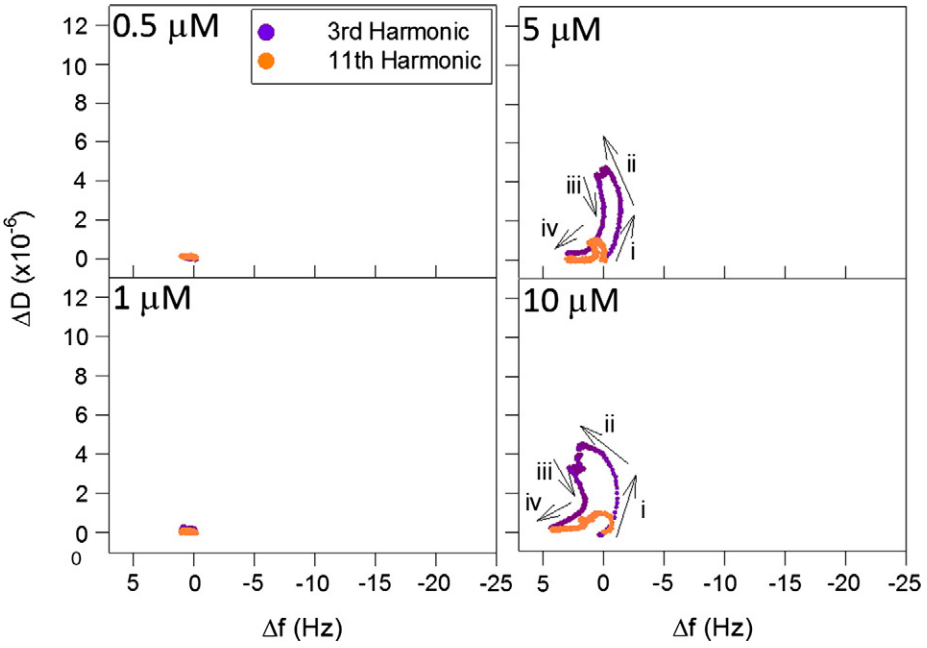

Fig. 4. Representative ΔD vs. Δf plots showing the action of alamethicin at 0.5, 1, 5, and 10 μM concentrations on a supported PC membrane. The arrows indicate the progression of data points over time. The changing directions of the arrows (i–iv) can be related to several different processes occurring in the membrane. The frequency axis has been reversed so that increases in mass are represented by frequency shifts to the right. Representative data from each peptide concentration were chosen from sets of at least 3 replicate experiments.

on the bilayer surface, Δf will be negative and large enough to be observable. Also included are the results for the dimeric state of SMAP-29 since there is the possibility of dimerization due to the presence of a terminal cysteine added to SMAP-29 tested in our work. For the SMAP-dimer, all states of interaction give rise to negative Δf and the magnitude is significantly large compared to all other cases considered in Table 2. These calculated maximum Δf estimates allow us to look at specific peptide induced changes on the bilayer in molecular terms.

3.2. Alamethicin prefers pore formation

The net changes in the frequency and the dissipation for the bilayer exposed to alamethicin are shown on Fig. 3 for various concentrations of alamethicin in the aqueous phase. For all alamethicin concentrations, the experimental data show that (i) the frequency changes are positive suggesting a net mass loss occurs, (ii) all overtones show uniform responses, suggesting a process that is homogeneous along the depth of the bilayer, and (iii) the dissipation changes are very small, indicating that the membrane retained the relatively rigid order similar to the unperturbed lipid bilayer. The mass loss and the uniform response at all overtones are consistent with alamethicin causing some amount of lipid molecules to be removed from the bilayer and creating cylindrical pores. The very small dissipation change is consistent with alamethicin occupying the pore walls to make the bilayer as rigid as its original state.

The dynamics of the interaction process are revealed by the ΔD vs. Δf plots in Fig. 4. As discussed by McCubbin et al. [52] and in a previous paper from our lab [49], these plots reveal the time dependent dynamic changes that occur in the membrane which are not captured by the plots of net changes in ΔD and Δf shown on Fig. 3. The direction of each line in the graphs in Fig. 4 can be related to different molecular scale mechanisms occurring in the membrane. The x-axis is scaled such that the frequency changes to the "east" would correspond with mass increases. At bulk solution concentrations of 0.5 μM and 1 μM alamethicin, the membrane did not show significant changes. At 5 μM, simultaneous increases in mass and dissipation occurred initially, which corresponded with a line moving in the north–east direction (labeled *i*). The data then shifted to the north–west direction (labeled *ii*), indicating that the viscoelasticity of the membrane was

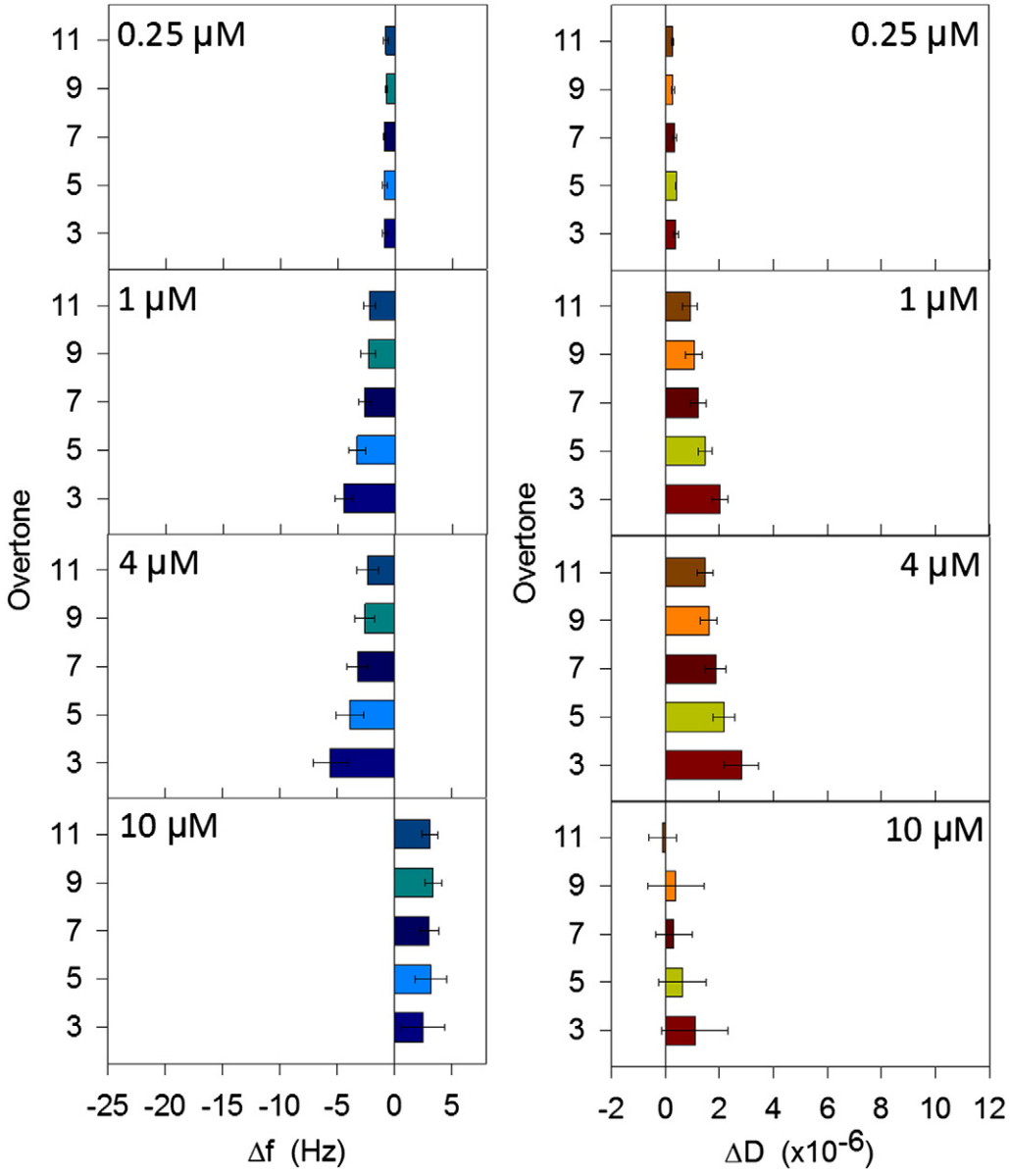

Fig. 5. Frequency and dissipation shifts for chrysophsin-3 (data previously published) [48]. Frequency changes at all overtones suggest insertion of the peptide into the membrane and greater decreases in frequency at the 3rd overtone are indicative of peptide adsorption to the bilayer surface.

still increasing, but mass had been lost. The bilayer then became more rigid with a small increase in mass and appreciable decrease in dissipation (labeled *iii*), followed again by mass loss (labeled *iv*). A similar phenomenon occurred at 10 μM alamethicin, but with larger changes in mass throughout the process and a faster initial rate of peptide adsorption to the membrane surface. These graphs showed that alamethicin first attached to the bilayer (mass addition) and caused the membrane to become more viscoelastic. The increasing "softness" of the bilayer could be due to decreasing organization of the membrane structure. The alamethicin then promotes pore formation in the bilayer, causing lipid removal and a more rigid bilayer structure as the peptides stabilized the edges of pores.

3.3. Chrysophsin-3 displays insertion, surface adsorption and pore formation

Chrysophsin-3 exhibited a concentration-dependent interaction mechanism on the PC bilayer (Fig. 5). At a concentration of 0.25 μM, Δf was negative and uniform at different overtones suggesting that a small amount of chrysophsin-3 was inserted into the membrane. Between 1 μM and 2 μM chrysophsin-3 (not shown), Δf was negative and the 3rd overtone showed a larger magnitude compared to the higher overtones suggesting that the peptide continued to insert into the membrane, but also was adsorbed on the bilayer surface. At 4 μM chrysophsin-3, the net Δf values and overtone responses were similar to that at 1 μM, indicating peptide insertion and surface adsorption. The dissipation changes were larger, however, suggesting that the peptide induced actions were perturbing the organization of the bilayer. At the largest chrysophsin-3 concentration of 10 μM, Δf became positive, overtone responses were more uniform, and the dissipation significantly decreased to small values, all suggesting that the net mass loss could be due to the formation of pores with the peptide stabilizing the pore walls and making the membrane reasonably rigid as in its unperturbed state.

The dynamics of the interactions between chrysophsin-3 and the PC bilayer displayed in the ΔD vs Δf plots in Fig. 6 show that at the low concentration no significant change occurred on the bilayer. However, for 1 μM and 4 μM concentrations, an initial shift in the north–east direction (*i*) indicated simultaneous increases in mass and membrane viscoelasticity as peptide attached to the membrane. The 3rd overtone showed greater change than the 11th overtone, suggesting that most of the peptide-membrane dynamics was taking place near the surface of the membrane. The graph then shifted to a south–west direction (*ii*), indicating that mass had been lost from the membrane, leaving a more structurally organized and rigid film that still contained more mass than the original lipid membrane before peptide exposure. The results at 10 μM showed the same trends, but revealed a larger initial mass addition to the membrane, followed also by a larger mass loss (*ii*), resulting in a more rigid film.

3.4. Indolicidin prefers surface adsorption

The QCM-D responses for indolicidin at different peptide concentrations are shown on Fig. 7. The QCM-D responses for 0.5 μM and 1 μM indolicidin were not strong, indicating some interactions but no significant changes to the membrane. At 5 μM indolicidin, frequency change was negative at the 3rd harmonic, but positive at higher overtones, suggesting that mass had been added to the bilayer surface, but removed from within the bilayer. These results showing both mass gain and loss may be explained by simultaneous peptide adsorption at the surface (corresponding to the negative frequency shift in the 3rd harmonic) and promoting some lipid loss from the bilayer (corresponding to the positive frequency shift at higher overtones). The dissipation changes also show significant positive values indicating that the membrane organization is somewhat disrupted because of the removal of lipids without accompanying space filling by the peptide. At the highest concentration of 10 μM indolicidin, the membrane experienced mass gain that was non-uniform at different overtones, the largest gain being in the 3rd overtone. This indicated significant surface adsorption of indolicidin with increasing concentration and partial peptide insertion into the membrane space where lipid molecules had been removed. The 10 μM indolicidin concentration also resulted in larger ΔD values and, therefore, the "softest" film compared to other indolicidin concentrations. The creation of a "softer" film suggests that the lipid bilayer has been disrupted, allowing more water to enter the membrane space since the inserted amount of peptide was probably small compared to the adsorbed amount of peptide.

The dynamics of indolicidin action on PC membranes as seen from the ΔD vs. Δf plot (Fig. 8) showed that the rate of peptide attachment

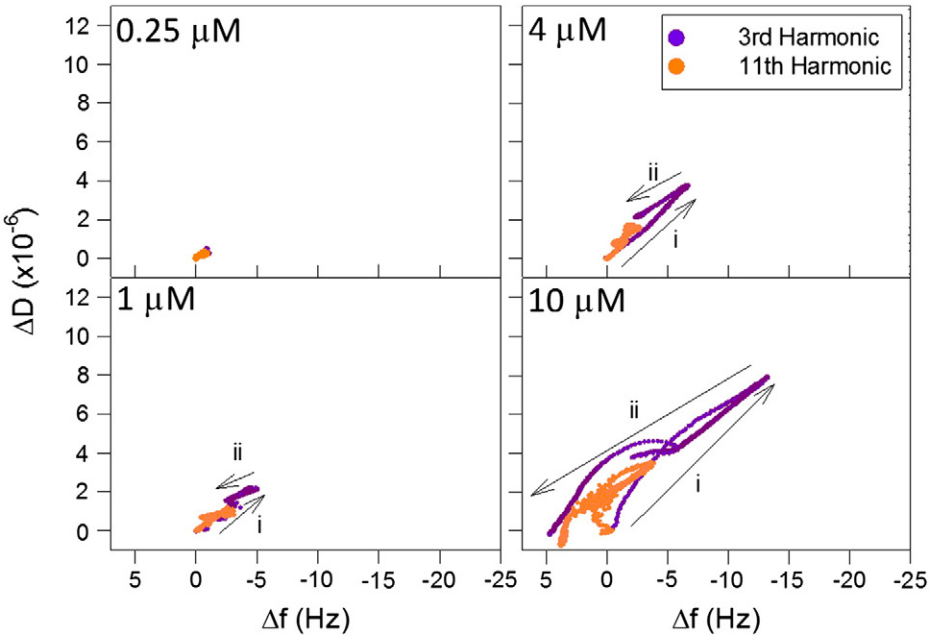

Fig. 6. Representative ΔD vs. Δf plots for chrysophsin-3 at 0.25, 1, 4, and 10 μM concentrations. The arrows reveal two distinct processes occurring in the membrane as a result of exposure to chrysophsin-3: (i) increasing mass and dissipation, due to peptide incorporation into the bilayer and (ii) simultaneous decreasing mass and dissipation.

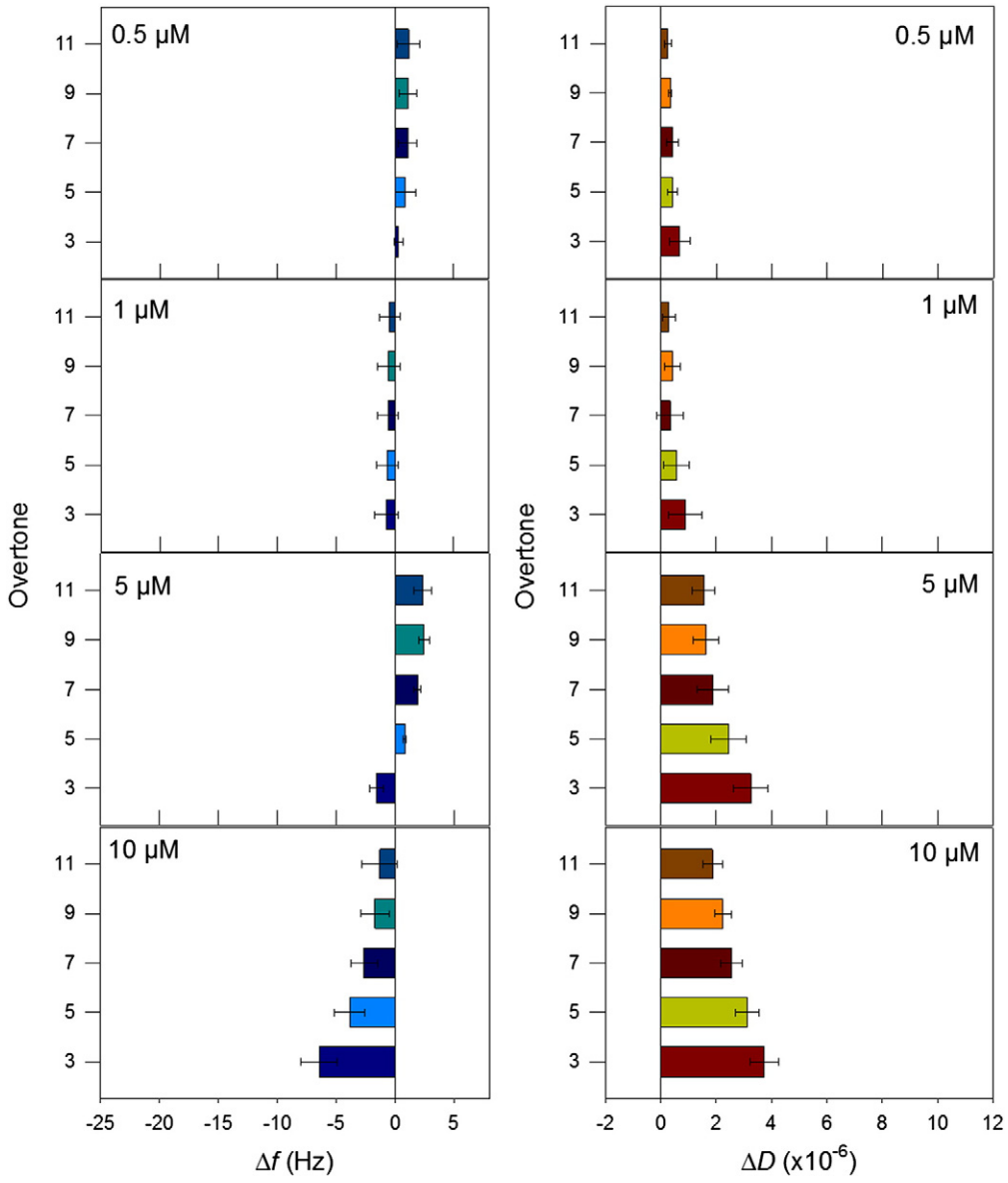

Fig. 7. Frequency and dissipation shifts resulting from indolicidin action on a supported PC bilayer at various peptide concentrations. The differences shown in each overtone indicate that the processes occurring throughout the membrane thickness are not uniform. The error bars represent the standard deviation based on at least 3 replicate experiments.

to the bilayer at the beginning of the process was higher than with alamethicin and chrysophsin-3 discussed earlier. This is revealed by the substantial separation of data points in the ΔD vs. Δf trace (since two adjacent frequency data points correspond to some fixed time interval, points separated by long distance indicate a rapid change of frequency compared to a situation where the points are very close to one another). The plot at 10 μM indolicidin indicated a higher rate of initial adsorption in the 3rd harmonic (*i*), followed by a slower loss of mass from the membrane (*ii*). Before the membrane stabilized during the 1-h incubation period with the peptide, the bilayer regained a small amount of mass and continued to decrease in dissipation (*iii*), indicating that the molecules within the membrane were becoming more ordered. The subsequent increases in dissipation and mass (*iv*) resulted from the start of buffer flow after incubation with the peptide. The mechanism then shifted to a loss in mass and dissipation (*v*) as the membrane lost weakly attached particles and began to stabilize.

3.5. SMAP-29 exhibits adsorption, insertion, pore formation and presence as dimer

For SMAP-29, significant changes in frequency or dissipation were not observed at or below the 1.0 μM concentration (Fig. 9). Between 2 μM and 10 μM peptide concentrations, large frequency decrease and dissipation increase occurred, that were not homogeneous over the various overtones. The negative shifts in frequency were larger at lower overtones and the largest Δf values were observed for 10 μM SMAP-29. These results indicate that more mass was added to the membrane surface than throughout the membrane thickness, suggesting that peptides were adsorbing as well as inserting into the bilayer. Pore formation is also possible but as the estimates in Table 2 show, the positive frequency change due to pore formation can be more than compensated by the negative frequency change associated with peptide insertion and surface adsorption.

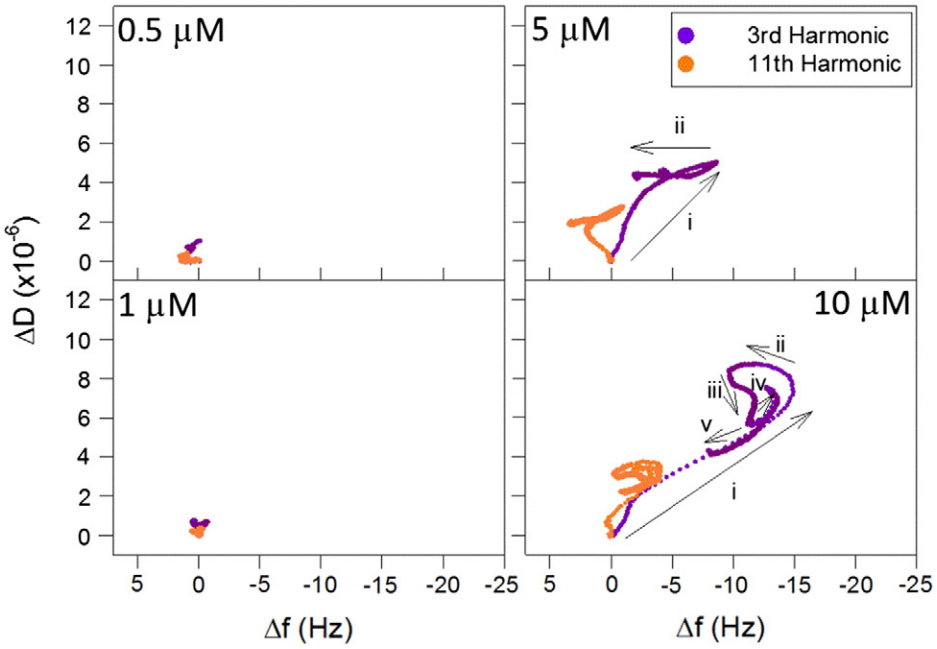

Fig. 8. Representative ΔD vs. Δf plots for indolicidin at 0.5, 1, 5, and 10 μM concentrations. The arrows show that the addition of peptide into the membrane (i) is followed by a series of more complex interactions (ii–v) as time progresses.

The frequency change for concentrations of 5 μM to 10 μM SMAP-29 was notably large, about −21 Hz at the 3rd overtone. The calculated maximum free energy changes in Table 2 for SMAP-29 are well below this value for all states of the peptide considered. Therefore, the large frequency shifts resulting from exposing the lipid bilayer to these concentrations of SMAP-29 require alternate molecular reasoning. The most likely explanation comes from the possible dimerization of SMAP-29 because of the formation of disulfide bonds between the terminal cysteine residues attached to the peptide. This phenomenon was reported previously in a study by Uzarski et al., in which cysteine-terminated cecropin-P1 peptide formed disulfide bonds, resulting in peptide dimmers [35]. The peptide dimer could still insert into the membrane or form a pore in the membrane but a significant portion of the dimer (almost 30 amino acid residues) would remain exposed to water on the bilayer surface.

Positive shifts in dissipation indicating a softer membrane were observed for all peptide concentrations with the largest ΔD values recorded for the third overtone. We noted that the SMAP dimers inserted into the bilayer or the dimers forming pores would have a significant part of them outside the bilayer membrane creating a water filled region crowded with the exposed parts of the dimers. Such a molecular system would make the effective membrane soft or viscoelastic and would give rise to the high dissipation changes observed.

The presence of dimerized SMAP-29 molecules could also explain the fast rate of initial mass attachment (*i*) to the lipid bilayer at 5–10 μM concentrations (Fig. 10). The membrane became substantially more viscoelastic upon this mass addition, suggesting that it was becoming more structurally disorganized. The rate of change slowed as peptide attachment reached a saturation point around $\Delta f = 18$ Hz for both concentrations and the membrane began to lose mass, while increasing in viscoelasticity (*ii*). During the final buffer rinse, the dissipation then continued to increase along with the membrane mass (*iii*). This suggests that the mass gain may stem from trapping of some buffer by the exposed parts of peptide dimer on the bilayer surface while the increase in dissipation or viscoelasticity may reflect a structural disorganization of a more hydrated, peptide containing region on the bilayer surface.

3.6. Comparison of kinetics of peptide–membrane interactions

We have used the QCM-D data to estimate some kinetic information about how the peptides interact with bilayer. The frequency response of the QCM-D traces show that when the peptide comes into contact with the bilayer, a significant change in the frequency occurs in the initial period of contact following time point denoted as t_2 in the experiment (see QCM-D time trace in Supplemental Information Topic S1). The duration of this initial period as well as the rate of change of frequency during this initial period are found to be different for the four peptides (Fig. 11). The duration of change for this initial period of contact is the smallest for alamethicin and largest for chrysophsin-3 and the other two peptides have comparable behaviors. The rate of mass or frequency change in this initial period is the largest for SMAP-29 and smallest for alamethicin and chrysophsin-3. Indolicidin exhibits an intermediate rate of change. We observe that the initial interaction times (duration of initial change) of the four peptides are better differentiated at lower peptide concentrations whereas the initial interaction rates (frequency change over time) of the four peptides are better differentiated at the higher peptide concentrations.

3.7. Calculated peptide molecular structural properties

Key peptide structural properties were calculated to establish a connection between the QCM-D results and the molecular processes they signify, with the molecular structural features of the peptides. The most common properties used to differentiate peptides in the literature are hydrophobicity, charge, and secondary structure. Many numerical scales of hydrophobicity Φ_n for each peptide residue *n* have been developed in the literature (see Supplemental Material Topic S3). Although they show some correlation with one another, the numerical measures can be very different. Therefore they are used more for the purposes of comparison. We have calculated the hydrophobicity of the four peptides using the normalized consensus scale of Eisenberg and the Urry scale based on phase inversion and the results are provided in Table 3 [54, 55]. The hydrophobicity of the entire peptide Φ ($=\sum \Phi_n$ for all $n = 1$ to N amino acids considered) and the hydrophobicity per residue N

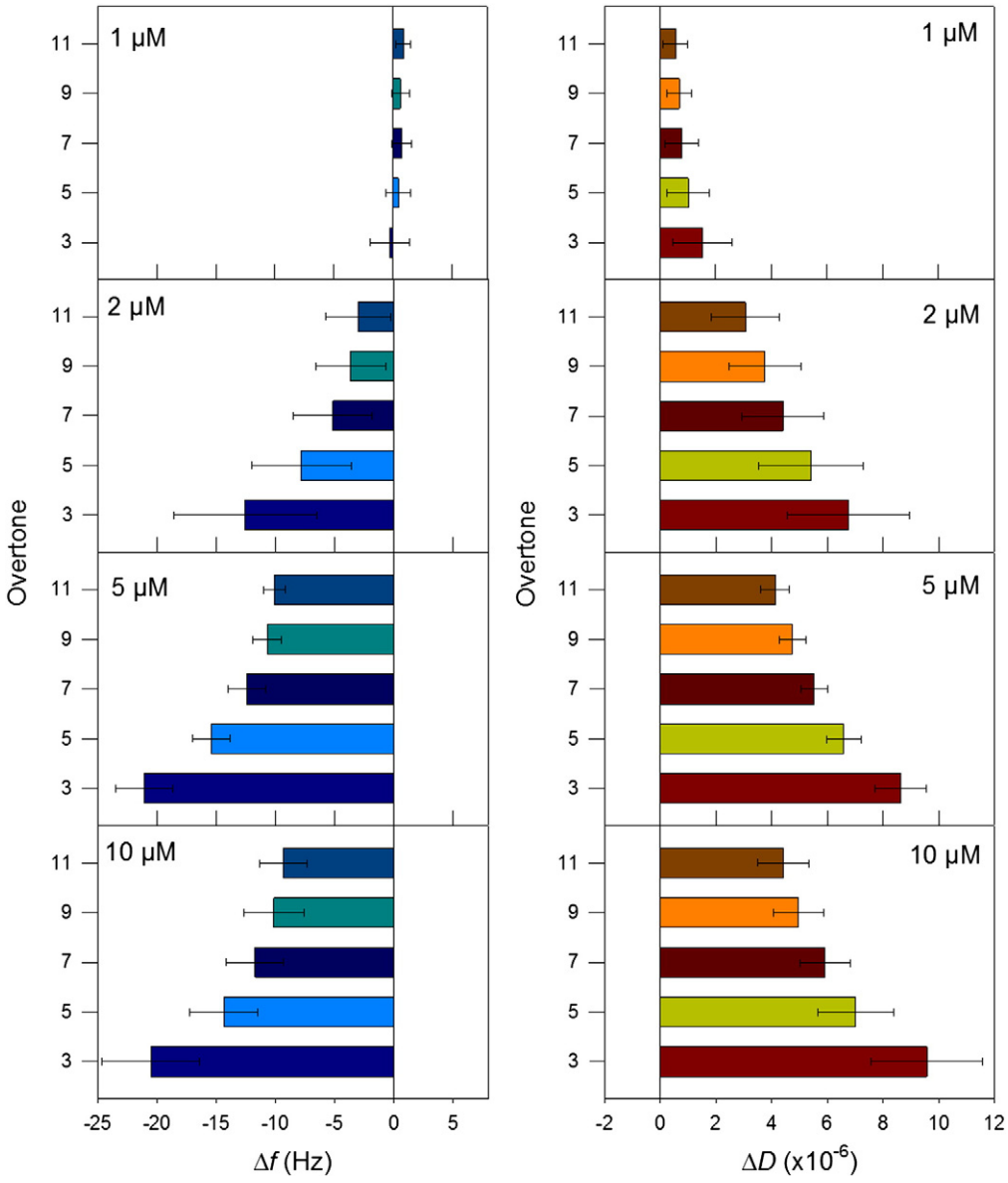

Fig. 9. Frequency and dissipation shifts resulting from SMAP-29's action on a supported PC bilayer at various peptide concentrations. The non-uniform changes at each overtone indicate that the interaction mechanism consists of a combination of peptide adsorption and insertion. Error bars represent the standard deviation based on at least 3 replicate experiments.

(Φ / N) are both shown. For alamethicin containing two unnatural amino acids, the hydrophobicity of aminoisobutyric acid (U) was taken to be the average of the chemically similar amino acids, alanine and valine, and the hydrophobicity for L-phenylalaninol (Z) was taken to be the same as for phenylalanine.

In the Urry scale that is based on hydrophobic association, indolicidin was the most hydrophobic (based both on the entire peptide and also on a per residue basis) and alamethicin was the least hydrophobic, because of the large hydrophobicity estimates for tryptophan compared to the small estimates for alanine and valine. In the Eisenberg consensus scale based on various transfer free energies, alamethicin was the most hydrophobic while SMAP-29 was hydrophilic, reflecting the total absence of charge on alamethicin and the presence of 11 charged groups on SMAP-29.

A second characteristic used for analyzing amino acid sequences of membrane-related proteins is the hydrophobic moment, a measure of the amphiphilicity of the peptide. It is calculated for an amino acid sequence of N residues, with residue n having the hydrophobicity Φ_n from the definition,

$$\mu_H = \{\Phi_n \cos(\delta n)\}^2 + \{\Phi_n \sin(\delta n)\}^{2^{1/2}} \quad (4)$$

where δ is the angle (in radians) at which successive side chains emerge from the backbone when the peptide is viewed down its axis. For an α-helix, this angle is 100°. The hydrophobic moment will be small for a helix where all residues are evenly distributed about the helix, and large for the case where most of the hydrophobic residues are on one side and most of the hydrophilic residues are on the other. Thus, the hydrophobic moment measures the extent of amphiphilicity of a helix. Any of the hydrophobicity scales could be used to provide the residue contributions Φ_n and we have used the Eisenberg consensus scale for this purpose. The calculated hydrophobicity moment per residue for all four peptides is also given in Table 3. The hydrophobic moment is the largest for alamethicin, indicating its preference for helical

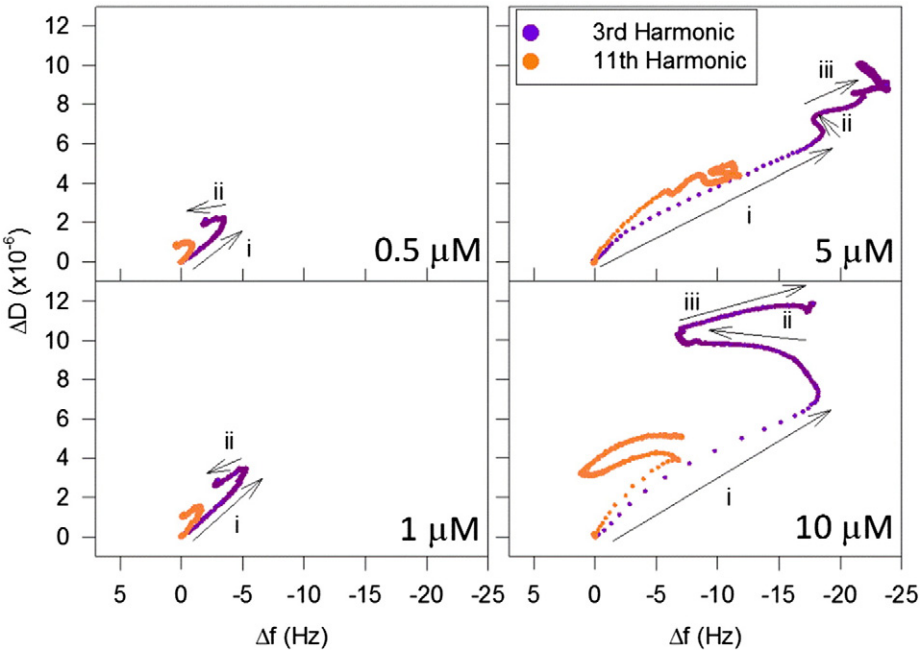

Fig. 10. Representative Δ*D* vs. Δ*f* plots for SMAP-29 at 0.5, 1, 5, and 10 μM concentrations. The spacing between the data points indicates that mass was added to the membrane at a faster rate than the other peptides, possibly due to the large mass of the dimerized SMAP-29 molecules.

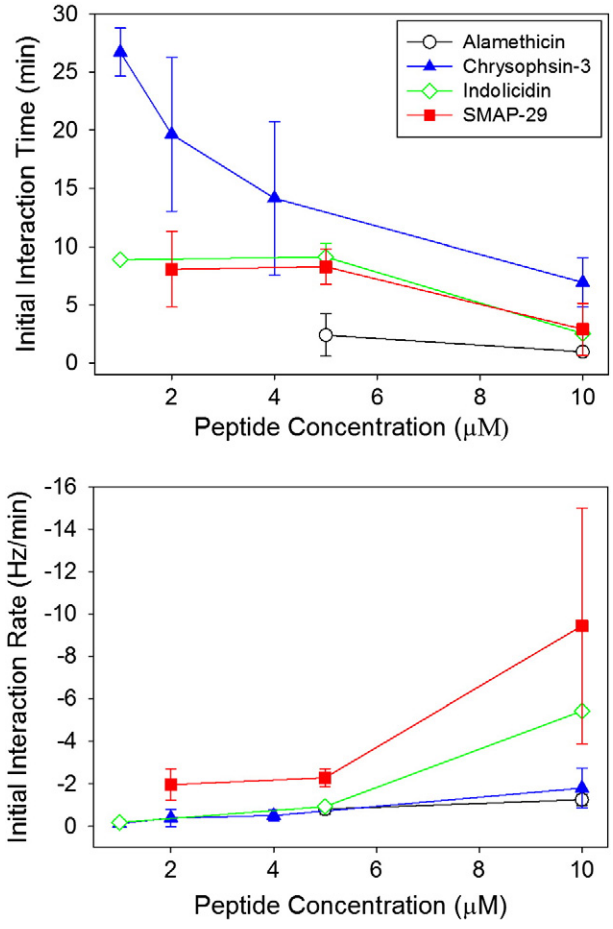

Fig. 11. Initial interaction times and rates for various AMP concentrations. These values represent the rate of change during the initial stage of contact between the bilayer and the peptide.

secondary structure, and is the smallest for indolicidin, indicating the low probability of a α-helix. Both chrysophsin-3 and SMAP-29 have intermediate values of hydrophobic moment indicating a larger likelihood of α-helices.

In contrast to the hydrophobicity scales established for amino acids based on experimental measurements of free energy change of some relevant processes (discussed in Supplemental Material Topic S3), methods based on data mining have also been developed to predict the hydrophobicity and amphiphilicity of polypeptides [56]. Artificial neural networks were trained on a set of experimentally solved protein structures to predict properties including the relative surface accessibility of the amino acids and the probability of having a given secondary structure. In this approach, a given amino acid does not have a fixed value for a property but it depends on where the amino acid occurs in the peptide chain. The solvent accessible surface area (ASA) of amino acid residues within a native folded protein is calculated by rolling a sphere the size of a water molecule over the protein surface. For comparative purposes, the ASA is transformed into a relative surface area, which is calculated as the ASA of a given amino acid residue in the polypeptide chain, relative to the one where the amino acid is in maximal possible exposure, with the residue in the center of a tri-peptide between either glycine or alanine residues. The neural networks were also trained on the same protein data set to learn the probability of a secondary structure for each amino acid depending on where it may occur in a polypeptide.

Using the web-based tool NetSurfP where these neural network calculations can be implemented, we have calculated and plotted the relative solvent accessible surface area for the four peptides in Fig. 12 and the probability of the residue being part of an α-helix in Fig. 13. Since this neural network learning is based on a protein data set with experimentally solved protein structures, no information on the non-natural amino acids are available. For the purposes of our calculations, we have used alanine and valine as replacements for aminoisobutyric acid and phenylalanine for phenylalaninol while calculating for alamethicin and have provided two sets of results corresponding to either alanine (A) or valine (V). The calculated results show a set of amino acids

Table 3
Hydrophobicity and hydrophobic moment of peptides.

Peptide	Urry hydrophobicity		Eisenberg hydrophobicity		Eisenberg hydrophobic moment per residue
	For whole peptide	Per residue	For whole peptide	Per residue	
Alamethicin	−30.7	−1.54	6.22	0.3110	0.3084
Chrysophsin-3	−41.5	−2.08	1.52	0.0762	0.1537
Indolicidin	−44.45	−3.42	0.29	0.0223	0.0795
SMAP-29	−40.95	−1.41	−5.25	−0.1810	0.1957

with larger surface accessibility and a set of amino acids with low surface accessibility for all peptides, suggesting the possibility of amphiphilic nature for their secondary structures. The fact that such facial segregation may not occur for indolicidin is likely due to the small number of amino acids present in it. The predicted probability of a residue having α-helical structure shown on Fig. 13 clearly indicates that alamethicin, chrysophsin-3 and SMAP-29 can all have α-helical secondary structures while indolicidin has a random coil secondary structure (calculated data for random coils and beta structure are not plotted on the figure).

3.8. Linking peptide molecular structure to membrane interactions

The calculated structural properties of hydrophobicity, accessible surface area and probability of α-helical secondary structures as well as the net charge on the peptide can be related to the molecular scale descriptions of peptide–membrane interactions derived from QCM-D measurements. In Fig. 14, we summarize the molecular scale models for peptide–bilayer interactions by combining the results obtained from the QCM-D experiments with the insights provided by the calculated peptide properties.

For alamethicin, the dominant molecular event suggested by QCM-D data is pore formation over the range of concentrations studied. Alamethicin is amphiphilic with α-helical structure as determined by the calculated hydrophobic moment, relative accessible surface area and the probability for α-helical secondary structure. It has zero charges on the surface. It has the largest hydrophobicity among the four peptides in the Eisenberg scale, which is based on the free energy of transfer water to a second bulk phase or to an interface. These molecular properties of alamethicin all promote its insertion into the bilayer creating pores, as part of the pore wall separating the lipid tails from water channels. Further, in the Urry scale which is based on hydrophobic association, the hydrophobicity of alamethicin is the smallest. That would suggest that it is less likely that alamethicin is inserted into the bilayer either as a single molecule or as an aggregate devoid of water channel, even though it cannot be ruled out.

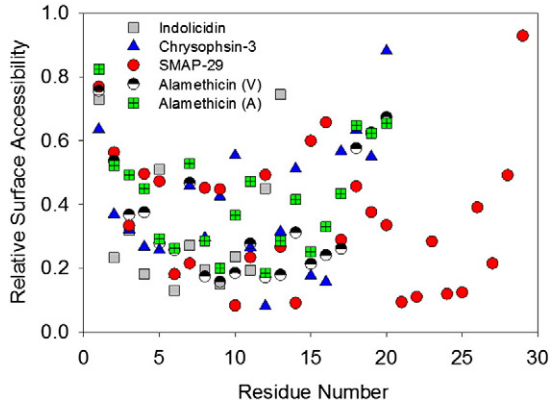

Fig. 12. Relative solvent accessible surface area of the amino acid residues in each peptide. Alanine (A) and valine (V) were used as replacements for aminoisobutyric acid and phenylalanine was substituted for phenylalaninol. These values were calculated using NetSurfP [56].

For chrysophsin-3, the dominant molecular events suggested by the QCM-D data include membrane insertion and pore formation, as well as surface adsorption. Chrysophsin-3 is amphiphilic with α-helical structure as shown by the calculated hydrophobic moment, relative surface accessibility and the probability for α-helical secondary structure. Therefore it is reasonable to expect its presence in the bilayer as a part of pores, similar to alamethicin. The five charges on chrysophsin-3 can contribute to attractive charge–dipole interactions with the zwitterionic head groups on the PC bilayer, thereby allowing the peptide to also be in the adsorbed state on the bilayer. At the same time, the charges are concentrated near the C-terminus and the rest of the peptide is significantly hydrophobic as measured by both the Urry and Eisenberg scales. Consequently, chrysophsin-3 can also just insert as a single molecule or as an aggregate into the bilayer.

In the case of indolicidin, the dominant molecular events suggested by the QCM-D data include surface adsorption and partial insertion into the bilayer. The peptide is not amphiphilic, does not have the α-helical secondary structure and is really a random coil. Therefore, indolicidin does not promote pore formation in the bilayer (at least over the peptide concentration range studied). The low probability of indolicidin being part of a pore wall separating hydrophobic tails of the lipid from water channels is also supported by the small magnitude of hydrophobicity on the Eisenberg scale. Indolicidin has four charges and has the largest hydrophobicity, among the four peptides, in the Urry scale because of the presence of the tryptophan residues. As a result it can strongly adsorb at the bilayer surface both through the attractive charge–dipole interactions as well as through hydrophobic association with the bilayer surface uncovered by the lipid head groups. Further, because of the hydrophobicity and the coil-like conformation, it can also partially insert itself into the bilayer.

For SMAP-29, the QCM-D experiments suggest significant surface adsorption and also pore formation. Also, there was clear indication that the sample SMAP-29 used which contained a C-terminus cysteine had dimerized (this would not be relevant in the case of SMAP-29 without the cysteine modification). The calculated hydrophobic moment, accessible surface area and probability of α-helical secondary structure are all consistent with the possibility of pore formation with the peptide being at the pore walls. The large number of 11 charges

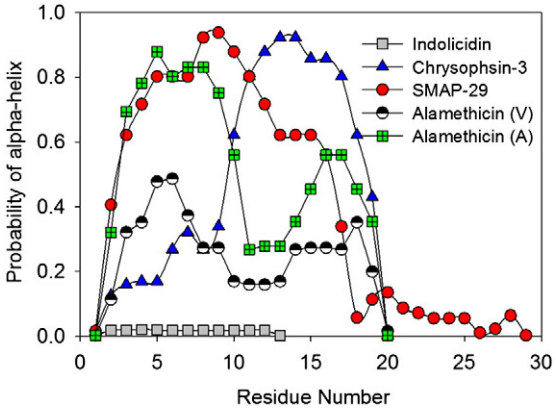

Fig. 13. Probability of amino acid residues having an α-helical structure. These values were calculated using NetSurfP [56].

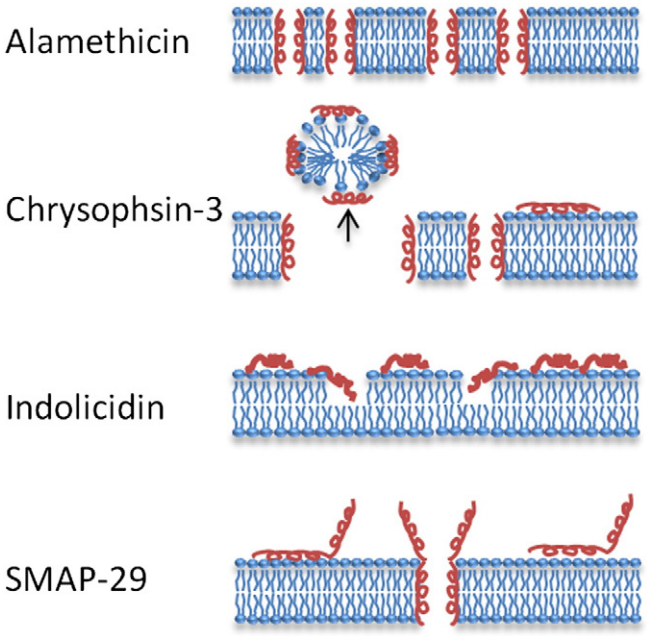

Fig. 14. Representative mechanistic models for alamethicin, chrysophsin-3, indolicidin, and SMAP-29 action on a supported PC membrane. AMPs and lipids are shown in red and blue, respectively.

on the peptide supports the idea of strong surface adsorption through attractive charge–dipole interactions as well as hydrophobic association. The significantly large mass changes observed in the QCM-D required consideration of the peptide dimers and could not be explained if dimerization had not occurred.

3.9. AMP concentrations marking QCM-D signatures span the range for bacterial inhibition and hemolysis

The AMP concentrations at which the QCM-D experiments showed peptide induced changes (0.25 μM–10 μM) were within the range of bacteria-inhibiting and hemolytic concentrations reported for these AMPs. In the QCM-D experiments, alamethicin exhibited substantial impact on the membrane at concentrations above 1 μM, which was within the range of LC_{50} (50% lethality concentration) values of 1.955 μM and 0.988 μM, respectively [57] reported for invertebrate models *Artemia salina* and *Daphnia magna* after a 36-h incubation with alamethicin. Chrysophsin-3, which exhibited measureable changes above 0.25 μM in the QCM-D experiments has been found to inhibit *Bacillus subtilis ATCC* 6633 and *Escherichia coli* WT-2 bacterial growth at 0.25 μM (minimum lethal concentration required to kill 99% of bacteria) and cause 50% hemolysis of human erythrocytes at around 2 μM [22]. Indolicidin created substantial changes in the PC membranes at concentrations above 1 μM in the QCM-D experiments that correlated with the Minimum Inhibitory Concentration (MIC) of 1 to 13 μM for various bacteria and hemolytic concentrations around 10 μM against rat erythrocytes in the literature [58]. For SMAP-29, MIC values between 0.5 μM and 2 μM for various bacteria and ~80 μM for 50% hemolysis of human erythrocytes have been reported [33]. These concentrations are larger than the concentrations that led to substantial changes in the PC membranes in the QCM-D experiments which could have been due to the dimerization of the cysteine containing peptide used.

4. Conclusions

The most interesting conclusion from this study is the recognition that QCM-D provides many unique signatures or fingerprints to differentiate the action of antimicrobial peptides on lipid bilayer membranes. The most obvious and easy to observe fingerprint was the static (actually the difference between two steady-state conditions which we have termed "static" for simplicity) net frequency change and net dissipation change caused solely by the peptide, at different overtones and at different peptide concentrations as shown on Figs. 3, 5, 7 and 9. Even if we had not been able to interpret these data in molecular mechanistic terms, there is no denying the obvious differences in the signatures shown by each of the four peptides. A second unique fingerprinting was provided by the dynamic Δf–ΔD plots, as shown on Figs. 4, 6, 8 and 10. Although not as obvious as the static data, these dynamic data also showed significant variations in the multistep interactions of the peptides with the bilayer. A third fingerprint was the data quantifying the initial stage of contact of the peptide with the bilayer as shown on Fig. 11. Changes in the membrane occurred quickly in the first stage followed by a slower process. Both the time duration of this first stage as well as the rate or intensity of change in this first stage were peptide-specific. We believe that it may be possible to identify yet other unique signatures by performing additional data mining of the rich steady state and dynamic measurements derived from the QCM-D experiments. By establishing a correlation between these unique fingerprints and peptide molecular properties for a sufficiently large database of peptide, we could potentially identify and/or design AMPs with good antimicrobial activity and low hemolytic activity for many biomedical applications.

Acknowledgments

This study was supported by funding from the Natick Soldier Research, Development & Engineering Center (NSRDEC), the Koerner Family Graduate Fellowship, and the Oak Ridge Institute for Science and Education (ORISE) Graduate Fellowship. We would like to thank Steve Arcidiacono (NSRDEC) for kindly providing the peptide SMAP-29 with cysteine termination, used in this study.

Appendix A. Supplemental material

See supplemental material for typical frequency and dissipation data obtained from QCM-D experiments (Figure S1). Calculations for the maximum frequency changes for various peptide interaction modes are presented and various hydrophobicity scales are also discussed and compared (Supplemental Material Topics S2 and S3). Supplementary data to this article can be found online at http://dx.doi.org/10.1016/j.bpc.2014.09.003.

References

[1] R.C. Skarnes, D.W. Watson, Antimicrobial factors of normal tissues and fluids, Bacteriol. Rev. 21 (1957) 273–294.
[2] E. Gazit, I.R. Miller, P.C. Biggin, M.S. Sansom, Y. Shai, Structure and orientation of the mammalian antibacterial peptide cecropin P1 within phospholipid membranes, J. Mol. Biol. 258 (1996) 860–870.
[3] K.A. Brogden, Antimicrobial peptides: pore formers or metabolic inhibitors in bacteria? Nat. Rev. Microbiol. 3 (2005) 238–250.
[4] A.K. Marr, W.J. Gooderham, R.E. Hancock, Antibacterial peptides for therapeutic use: obstacles and realistic outlook, Curr. Opin. Pharmacol. 6 (2006) 468–472.
[5] J.P. Powers, R.E. Hancock, The relationship between peptide structure and antibacterial activity, Peptides 24 (2003) 1681–1691.
[6] Y. Shai, Mode of action of membrane active antimicrobial peptides, Biopolymers 66 (2002) 236–248.
[7] L.M. Harriss, B. Cronin, J.R. Thompson, M.I. Wallace, Imaging multiple conductance states in an alamethicin pore, J. Am. Chem. Soc. 133 (2011) 14507–14509.
[8] R. Latorre, C.G. Miller, S. Quay, Voltage-dependent conductance induced by alamethicin–phospholipid conjugates in lipid bilayers, Biophys. J. 36 (1981) 803–809.
[9] H.W. Huang, Molecular mechanism of antimicrobial peptides: the origin of cooperativity, Biochim. Biophys. Acta 1758 (2006) 1292–1302.
[10] M. Dathe, T. Wieprecht, Structural features of helical antimicrobial peptides: their potential to modulate activity on model membranes and biological cells, Biochim. Biophys. Acta 1462 (1999) 71–87.
[11] S.E. Blondelle, R.A. Houghten, Probing the relationships between the structure and hemolytic activity of melittin with a complete set of leucine substitution analogs, Pept. Res. 4 (1991) 12–18.

[12] S.E. Blondelle, R.A. Houghten, Hemolytic and antimicrobial activities of the twenty-four individual omission analogues of melittin, Biochemistry 30 (1991) 4671–4678.
[13] S.E. Blondelle, R.A. Houghten, Design of model amphipathic peptides having potent antimicrobial activities, Biochemistry 31 (1992) 12688–12694.
[14] P. Juvvadi, S. Vunnam, E.L. Merrifield, H.G. Boman, R.B. Merrifield, Hydrophobic effects on antibacterial and channel-forming properties of cecropin A-melittin hybrids, J. Pept. Sci. 2 (1996) 223–232.
[15] R.P. Mee, T.R. Auton, P.J. Morgan, Design of active analogues of a 15-residue peptide using D-optimal design, QSAR and a combinatorial search algorithm, J. Pept. Res. 49 (1997) 89–102.
[16] R. Bessalle, A. Gorea, I. Shalit, J.W. Metzger, C. Dass, D.M. Desiderio, M. Fridkin, Structure–function studies of amphiphilic antibacterial peptides, J. Med. Chem. 36 (1993) 1203–1209.
[17] N. Ohmori, T. Niidome, T. Hatakeyama, H. Mihara, H. Aoyagi, Interaction of alpha-helical peptides with phospholipid membrane: effects of chain length and hydrophobicity of peptides, J. Pept. Res. 51 (1998) 103–109.
[18] K. He, S.J. Ludtke, W.T. Heller, H.W. Huang, Mechanism of alamethicin insertion into lipid bilayers, Biophys. J. 71 (1996) 2669–2679.
[19] H.W. Huang, Y. Wu, Lipid–alamethicin interactions influence alamethicin orientation, Biophys. J. 60 (1991) 1079–1087.
[20] C.E. Meyer, F. Reusser, A polypeptide antibacterial agent isolated from *Trichoderma viride*, Experientia 23 (1967) 85–86.
[21] A. Kessel, D.S. Cafiso, N. Ben-Tal, Continuum solvent model calculations of alamethicin–membrane interactions: thermodynamic aspects, Biophys. J. 78 (2000) 571–583.
[22] N. Iijima, N. Tanimoto, Y. Emoto, Y. Morita, K. Uematsu, T. Murakami, T. Nakai, Purification and characterization of three isoforms of chrysophsin, a novel antimicrobial peptide in the gills of the red sea bream, Eur. J. Biochem. 270 (2003) 675–686.
[23] A.J. Mason, P. Bertani, G. Moulay, A. Marquette, B. Perrone, A.F. Drake, A. Kichler, B. Bechinger, Membrane interaction of chrysophsin-1, a histidine-rich antimicrobial peptide from red sea bream, Biochemistry 46 (2007) 15175–15187.
[24] M.E. Selsted, M.J. Novotny, W.L. Morris, Y.Q. Tang, W. Smith, J.S. Cullor, Indolicidin, a novel bactericidal tridecapeptide amide from neutrophils, J. Biol. Chem. 267 (1992) 4292–4295.
[25] J.C. Hsu, C.M. Yip, Molecular dynamics simulations of indolicidin association with model lipid bilayers, Biophys. J. 92 (2007) L100–L102.
[26] C. Subbalakshmi, N. Sitaram, Mechanism of antimicrobial action of indolicidin, FEMS Microbiol. Lett. 160 (1998) 91–96.
[27] C.H. Hsu, C. Chen, M.L. Jou, A.Y. Lee, Y.C. Lin, Y.P. Yu, W.T. Huang, S.H. Wu, Structural and DNA-binding studies on the bovine antimicrobial peptide, indolicidin: evidence for multiple conformations involved in binding to membranes and DNA, Nucleic Acids Res. 33 (2005) 4053–4064.
[28] H. Khandelia, Y.N. Kaznessis, Cation–pi interactions stabilize the structure of the antimicrobial peptide indolicidin near membranes: molecular dynamics simulations, J. Phys. Chem. B 111 (2007) 242–250.
[29] A. Rozek, C.L. Friedrich, R.E. Hancock, Structure of the bovine antimicrobial peptide indolicidin bound to dodecylphosphocholine and sodium dodecyl sulfate micelles, Biochemistry 39 (2000) 15765–15774.
[30] I. Ahmad, W.R. Perkins, D.M. Lupan, M.E. Selsted, A.S. Janoff, Liposomal entrapment of the neutrophil-derived peptide indolicidin endows it with in vivo antifungal activity, Biochim. Biophys. Acta 1237 (1995) 109–114.
[31] F. Neville, A. Ivankin, O. Konovalov, D. Gidalevitz, A comparative study on the interactions of SMAP-29 with lipid monolayers, Biochim. Biophys. Acta 1798 (2010) 851–860.
[32] D. Raventos, O. Taboureau, P.H. Mygind, J.D. Nielsen, C.P. Sonksen, H.H. Kristensen, Improving on nature's defenses: optimization & high throughput screening of antimicrobial peptides, Comb. Chem. High Throughput Screen. 8 (2005) 219–233.
[33] R.M. Dawson, C.Q. Liu, Cathelicidin peptide SMAP-29: comprehensive review of its properties and potential as a novel class of antibiotics, Drug Dev. Res. 70 (2009) 481–498.
[34] S.Y. Shin, E.J. Park, S.T. Yang, H.J. Jung, S.H. Eom, W.K. Song, Y. Kim, K.S. Hahm, J.I. Kim, Structure–activity analysis of SMAP-29, a sheep leukocytes-derived antimicrobial peptide, Biochem. Biophys. Res. Commun. 285 (2001) 1046–1051.
[35] J.R. Uzarski, A. Tannous, J.R. Morris, C.M. Mello, The effects of solution structure on the surface conformation and orientation of a cysteine-terminated antimicrobial peptide cecropin P1, Colloids Surf. B: Biointerfaces 67 (2008) 157–165.
[36] S. Arcidiacono, P. Pivarnik, C.M. Mello, A. Senecal, Cy5 labeled antimicrobial peptides for enhanced detection of *Escherichia coli* O157:H7, Biosens. Bioelectron. 23 (2008) 1721–1727.
[37] P. Mueller, D.O. Rudin, Action potentials induced in bimolecular lipid membranes, Nature (London) 217 (1968) 713–719.
[38] R.O. Fox Jr., F.M. Richards, A voltage-gated ion channel model inferred from the crystal structure of alamethicin at 1.5-A resolution, Nature 300 (1982) 325–330.
[39] V. Rizzo, S. Stankowski, G. Schwarz, Alamethicin incorporation in lipid bilayers: a thermodynamic study, Biochemistry 26 (1987) 2751–2759.
[40] K. He, S.J. Ludtke, D.L. Worcester, H.W. Huang, Neutron scattering in the plane of membranes: structure of alamethicin pores, Biophys. J. 70 (1996) 2659–2666.
[41] S. Qian, W. Wang, L. Yang, H.W. Huang, Structure of the alamethicin pore reconstructed by X-ray diffraction analysis, Biophys. J. 94 (2008) 3512–3522.
[42] P. Wessman, M. Morin, K. Reijmar, K. Edwards, Effect of alpha-helical peptides on liposome structure: a comparative study of melittin and alamethicin, J. Colloid Interface Sci. 346 (1) (2010) 127–135.
[43] P. Pieta, J. Mirza, J. Lipkowski, Direct visualization of the alamethicin pore formed in a planar phospholipid matrix, Proc. Natl. Acad. Sci. U. S. A. 109 (2012) 21223–21227.
[44] D.P. Tieleman, H.J. Berendsen, M.S. Sansom, An alamethicin channel in a lipid bilayer: molecular dynamics simulations, Biophys. J. 76 (1999) 1757–1769.
[45] D.L. Parton, E.V. Akhmatskaya, M.S.P. Sansom, Multiscale simulations of the antimicrobial peptide maculatin 1.1: water permeation through disordered aggregates, J. Phys. Chem. B 116 (2012) 8485–8493.
[46] M.V. Voinova, M. Rodahl, M. Jonson, B. Kasemo, Viscoelastic acoustic response of layered polymer films at fluid–solid interfaces: continuum mechanics approach, Phys. Scr. 59 (1999) 391–396.
[47] A. Mechler, S. Praporski, K. Atmuri, M. Boland, F. Separovic, L.L. Martin, Specific and selective peptide–membrane interactions revealed using quartz crystal microbalance, Biophys. J. 93 (2007) 3907–3916.
[48] K.F. Wang, R. Nagarajan, C.M. Mello, T.A. Camesano, Characterization of supported lipid bilayer disruption by chrysophsin-3 using QCM-D, J. Phys. Chem. B 115 (2011) 15228–15235.
[49] K.F. Wang, R. Nagarajan, T.A. Camesano, Antimicrobial peptide alamethicin insertion into lipid bilayer: a QCM-D exploration, Colloids Surf. B: Biointerfaces 116 (2014) 472–481.
[50] C.A. Keller, B. Kasemo, Surface specific kinetics of lipid vesicle adsorption measured with a quartz crystal microbalance, Biophys. J. 75 (1998) 1397–1402.
[51] C.A. Keller, K. Glasmastar, V.P. Zhdanov, B. Kasemo, Formation of supported membranes from vesicles, Phys. Rev. Lett. 84 (2000) 5443–5446.
[52] G.A. McCubbin, S. Praporski, S. Piantavigna, D. Knappe, R. Hoffmann, J.H. Bowie, F. Separovic, L.L. Martin, QCM-D fingerprinting of membrane-active peptides, Eur. Biophys. J. 40 (2011) 437–446.
[53] S.E. Blondelle, K. Lohner, M. Aguilar, Lipid-induced conformation and lipid-binding properties of cytolytic and antimicrobial peptides: determination and biological specificity, Biochim. Biophys. Acta 1462 (1999) 89–108.
[54] D. Eisenberg, Three-dimensional structure of membrane and surface proteins, Annu. Rev. Biochem. 53 (1984) 595–623.
[55] D.W. Urry, The change in Gibbs free energy for hydrophobic association: derivation and evaluation by means of inverse temperature transitions, Chem. Phys. Lett. 399 (2004) 177–183.
[56] B. Petersen, T.N. Petersen, P. Andersen, M. Nielsen, C. Lundegaard, A generic method for assignment of reliability scores applied to solvent accessibility predictions, BMC Struct. Biol. 9 (2009) 51.
[57] M. Favilla, L. Macchia, A. Gallo, C. Altomare, Toxicity assessment of metabolites of fungal biocontrol agents using two different (*Artemia salina* and *Daphnia magna*) invertebrate bioassays, Food Chem. Toxicol. 44 (2006) 1922–1931.
[58] C. Subbalakshmi, V. Krishnakumari, R. Nagaraj, N. Sitaram, Requirements for antibacterial and hemolytic activities in the bovine neutrophil derived 13-residue peptide indolicidin, FEBS Lett. 395 (1996) 48–52.